EXPERIMENTAL RESEARCH OF AERODYNAMICS ON AN SST CONFIGURATION WITH HIGH LIFT DEVICES

Dong Youn KWAK*, Kenichi RINOIE** and Masayoshi NOGUCHI*
* Japan Aerospace Exploration Agency, Tokyo, 181-0015, JAPAN,
**Department of Aeronautics and Astronautics, University of Tokyo, 113-8656, JAPAN

Keywords: *Supersonic transport, High lift devices, Rolling moment, Ground effect*

Abstract

Low-speed and high angle of attack aerodynamics have been investigated to improve the take-off and landing performance of the Supersonic Transport (SST) configuration. Wind tunnel tests were conducted on an SST model with leading-edge flaps and trailing-edge flaps. The flap performances on 1) the lift-to-drag ratio, 2) the rolling moment characteristics and 3) the ground effect were investigated. The aerodynamic forces and the surface pressure were measured. A stereoscopic PIV survey was also performed to understand the flow fields. When the leading edge and trailing edge flaps are deflected simultaneously, obvious improvement of the lift-to-drag ratio was observed. This benefit is larger than the sum of each benefit when the leading edge flap and the trailing edge flap are deflected independently. Different rolling moment characteristics were observed on the configuration at high incidence angles, whereas linear and statically stable rolling moment characteristics were obtained for all configurations with and without flap deflections at low incidence angles. The flap performances were also investigated on the SST configuration when the model is located near the ground to simulate the take-off and landing phases. The results showed that static stability of the rolling moment characteristic is increased due to the ground effect.

Nomenclature

b = local semi span length, m
$b_{\max}$ = wing maximum semi span length, m
C_D = drag coefficient referred to stability axis
C_L = lift coefficient referred to stability axis
C_m = pitching moment coefficient referred to body axis non-dimensionalized using c_{mac}
c_{mac} = wing mean aerodynamic chord length, m
C_p = pressure coefficient
c_r = wing root chord length at model center line, m
C_{rol} = rolling moment coefficient referred to body axis non-dimensionalized using full span length
h = z-direction distance from the 0.25 c_{mac} to the ground, m
Re = Reynolds number based on c_{mac}
u = x-direction flow velocity of the body axis, m/s
U_∞ = freestream velocity, m/s
v = y-direction flow velocity of the body axis, m/s
w = z-direction flow velocity of the body axis, m/s
x = chordwise coordinate measured from apex of the wing at model center line, m
y = spanwise coordinate measured orthogonal to x from model center line, m
z = vertical coordinate measured orthogonal to x from model center line, m
α = angle of attack, degree
σ = incidence angle, degree (an angle that is composed from the direction of the free stream and the x-direction of the body axis)

ϕ = roll angle, degree (clockwise direction is positive when seen from downstream of the model)

Λ = sweep back angle, degree

1 Introduction

A research for the next generation super-sonic transport (SST) named NEXST (National Experimental Supersonic Transport) program has been conducted at JAXA (Japan Aerospace Exploration Agency) [1]. The NEXST program consists of a supersonic flight test project and fundamental research activities of the future SST technologies [2]. One of the fundamental research issues is to improve the aerodynamic performance of SST at take-off and landing. In general, the conventional SST has highly swept and low aspect ratio wing such as delta or double delta configurations. These SST wings have low lift and low lift-to-drag ratio characteristics as compared with those of the conventional subsonic aircraft. Therefore, applications of the high lift devices are considered as those improving the take-off and landing performances for SST. Single leading-edge (vortex) flaps and single trailing-edge flaps are thought to be the most feasible and reasonable devices for this purpose. In this paper, performances of the leading-edge flaps and the trailing-edge flaps for the SST configuration are investigated on the following three items.

- *Lift-to-drag ratio*
- *Rolling moment characteristics*
- *Ground effects*

The leading-edge flaps and the leading-edge vortex flaps can improve the lift-to-drag ratio at high angle of attack, because these devices actively control the leading-edge separation vortices [3]. The trailing-edge flaps enhance wing camber effects, and then induce the lift increment. When the leading-edge and trailing-edge flaps are deflected simultaneously, effect of both flaps combines each other. Hence, synergy of these effects is induced. One of the objectives of this paper is to make clear of the improvement of the lift-to-drag ratio due to the leading-edge and trailing-edge flaps of the SST configuration.

Self-induced roll oscillation called as "wing rock" is often observed on the delta configuration wings at high incidence angle [4]. This oscillation is an unsteady behavior induced by the leading-edge separation vortices. The nonlinear and abrupt change of the rolling moment are also observed originating from the nonlinear aerodynamic phenomena such as a vortex breakdown [5-7] and a vortex lift off [8,9]. Even if the wing is statically rolled, these behaviors affect the wing characteristics. The second objective of this paper is to clarify the static roll characteristics of the SST configuration with leading-edge and trailing-edge flaps.

The behavior of leading-edge separation vortices and hence the aerodynamic characteristics of the delta wing are influenced when the wing is at ground proximity for take-off and landing phase [10]. The characteristics of the leading-edge and trailing-edge flaps will also be affected by the ground proximity. In this paper, the ground effects of the SST configuration are also investigated.

Here, force and surface pressure measurements were made on the SST configuration model with different flap deflection angles at a Reynolds number based on the mean aerodynamic chord of 9.2×10^5. A stereoscopic PIV survey was also performed to understand the flowfields over the wing.

In summary, the purpose of this study is to discuss the improvements of take-off and landing performances of the SST configuration by making clear of the low speed and high alpha aerodynamic characteristics, rolling moment characteristics and ground effects.

2 Experimental Details

Figure 1 shows an SST model that was preliminarily designed by the second design phase of the NEXST program [2]. This SST configuration model consists of a cranked arrow wing and a fuselage. A kink is located at $y/b_{max}=0.55$ that connects the inboard wing of

Λ=66° sweep back angle and the outboard wing of Λ=42° sweep back angle. The wing has a warped wing section designed by the supersonic lifting surface theory to optimize the twist and camber distributions at a design Mach number of 1.7. The SST model has static pressure tappings on the upper surface of the left wing at x/c_r=0.55 and 0.83, as shown in Fig. 1. Further details of the wing cross section are described in reference 11. The wing has the inboard leading-edge vortex flap on the inboard wing, the outboard leading-edge flap on the outboard wing and the trailing-edge flap on the inboard wing [12]. The tested inboard leading edge vortex flap deflection angles are δ_{LE-in}=0°, 15° and 30° which are defined as the angle measured in the plane that is normal to the hinge line (see Fig. 1). The outboard leading edge flap deflection angles are δ_{LE-out} =0°, 5 and 12.2° which are defined as the angle measured parallel to x-direction. The trailing-edge flap deflection angles are δ_{TE} =0°, 10° and 30° which are defined as the angle measured parallel to x-direction.

Examples of the notation used in this paper are as follows. The notation *S301210* means the sharp leading-edge flap section with δ_{LE-in}=30°, δ_{LE-out}=12.2° and δ_{TE} =10°. A First digit of this notation ("*S*") means the shape of the leading-edge on the inboard wing. In this paper, results of sharp leading-edge flap section are discussed. Rounded ("*R*") leading-edge flap sections were reported in reference [11]. The 2nd and 3rd digits of this notation mean the deflection angle of the inboard leading edge vortex flap. The 4th and 5th digits of the notation mean the outboard leading edge flap deflection angle. The 6th and 7th digits mean the trailing-edge deflection angle. In the present tests, aerodynamic characteristics were investigated for each flap deflected separately or simultaneously.

The experiments were conducted in a 2×2m low speed wind tunnel (LWT2) and a 6.5×5.5m low speed wind tunnel (LWT) at JAXA, Japan. Wind tunnel tests for the ground effects were conducted in the LWT to secure large distance from the model to the ground that is desirable for the research of the ground
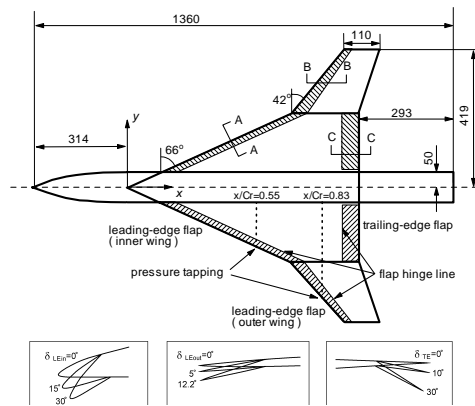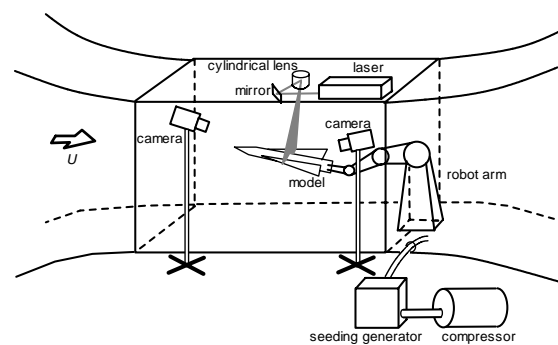

Fig.1 Schematics of the SST model

Fig.2 Schematics of PIV set up (seen from the port side) at 2× 2m low speed wind tunnel (LWT2)
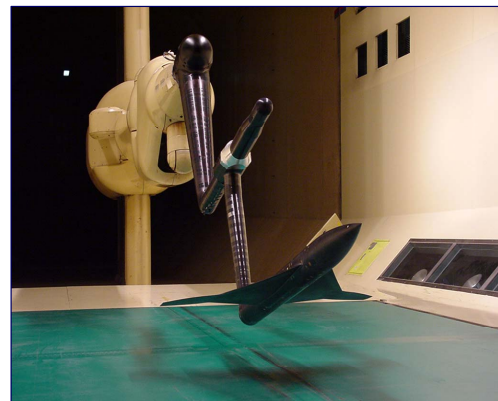

Fig.3 Ground effects test at 6.5× 5.5m low speed wind tunnel (LWT)

effects. Other tests were conducted in the LWT2. The freestream velocity was U_∞=30m/s and the Reynolds number based on the mean aerodynamic chord was Re=9.21×10^5. A schematic of the wind tunnel tests in the LWT2 is shown in Fig. 2. The SST model was

supported by an industrial multi-purpose robot-arm via a sting [13]. The rolling moment characteristics were investigated when the model was rotated to a roll direction at a fixed incidence angle σ [14]. Figure 3 shows the scene of the ground effect tests at LWT. The height of the SST model from the ground was decreased statically by use of the industrial multi-purpose robot-arm. A moving belt system was installed on the test section floor to eliminate the boundary layer developed along the wind tunnel wall [15].

Aerodynamic forces were measured by means of a six-component internal balance. The definition of the rolling moment is based on the body axis. Electronic scanning pressure sensors were used to measure the surface static pressure distributions. The force data measured from the internal balance were obtained by averaging 500 sampled data recorded at 2msec intervals. Pressure data were obtained by averaging 100 sampled data at 5msec intervals. The estimated overall uncertainties of the force and moment coefficients and the pressure coefficient C_P are less than ±0.5% and ±2% at 20:1 odds.

Stereoscopic PIV surveys were performed to understand the overall behavior of flow at x/c_r=0.55 and 0.83 on the upper surface. The PIV system (Fig.2) mainly consists of double-pulse

Nd:YAG lasers of 200mJ/pulse to illuminate the seeding particles in the flow, two CCD cameras with 1280×1024 pixels to acquire images of the illuminated particles, and a PC to control the equipment and to conduct data processing. Detailed information on the present PIV system is described in reference [16]. The laser light sheet illuminates the seeding particles over the upper surface of the model, which is parallel to the y-z plane based on the model body axis. Two CCD cameras, located at the port side of the test section, acquired instantaneous two laser sheets of particle images at 30μsec time intervals. Three component velocities (u, v, w) were calculated from images captured by the two CCD cameras. The averaged flow velocity vector distributions were obtained by averaging 300-900 sheets of instantaneous velocity vector images with an acquisition rate of 2Hz. The estimated overall uncertainty of the averaged velocity by PIV measurements is less than ±10% at 20:1 odds.

3 Results and Discussion

3.1 Lift-to-Drag Ratio Improvements

The flap performances on the longitudinal aerodynamics are briefly discussed in this section. Figure 4 shows the longitudinal aerodynamic characteristics of the baseline configuration (no flaps deflection; *S000000*), the configuration of the inboard and outboard leading-edge flaps deflection at the same time (*S301200*), that of the trailing-edge flap deflection (*S000010*), and finally for the combination of the leading-edge flaps and the trailing-edge flap deflection (*S301210*). The C_L vs. α curves in Fig.4(a) shows that the *S301200* slightly decreases C_L as compared with the *S000000*. However, obvious decrement of the C_D is observed for the *S301200* as compared with the *S000000* in Fig.4(b). The C_D reduction on the *S301200* induces improvements of the lift-to-drag ratio at C_L greater than 0.2 as compared with the *S000000* (Fig.4(d)). The tailing-edge flap (*S000010*) induces significant increase in the C_L, and increase in the C_D.
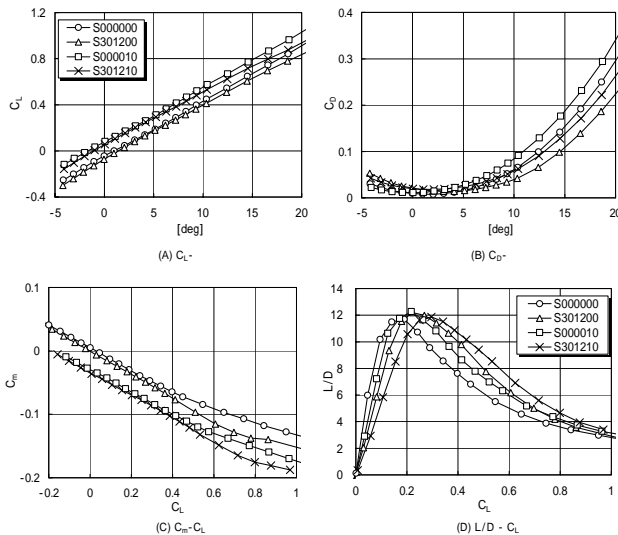

Fig.4 Longitudinal aerodynamic characteristics with the leading-edge and the trailing-edge flap deflection

Hence, the *S000010* improves the lift-to-drag ratio as compared with the *S000000*. The trailing-edge flap increases the nose-down pitching moment as compared with the *S000000*, while no obvious increments of the pitching moment are observed on the *S301200* (Fig.4(c)). When the leading-edge and trailing-edge flaps are deflected at the same time (*S301210*), higher lift-to-drag ratio is obtained on the *S301210* when compared with other three configurations at $C_L > 0.3$. It is suggested that the benefit of the *S301210* is composed by the sum of each benefit of the leading-edge flaps (*S301200*) and the trailing-edge flap (*S000010*). To understand this synergy effect of the leading-edge and trailing-edge flaps, Figure 5 shows the *L/D* vs. C_L curves on the *S301210* (triangular symbols), and that was obtained by the sum of each flap benefits (*S301200* and *S000010*; rectangular symbols. Linear effects of flap deflection were assumed to obtain these components). The *L/D* curve on the *S301210* is higher than that on the sum of the each flap benefits. The improvement of the *L/D* on the *S301210* as compared with the sum of each flap benefit (*S301200* and *S000010*) is a synergy effect induced by the leading-edge and trailing-edge flaps deflected at the same time. Detail mechanism of the synergy effects of the leading-edge and trailing-edge flaps were described in reference [17]. It was suggested that the benefit of the leading-edge flaps are depended on the angles of attack. The trailing-edge flap increases the effective angles of attack due to the camber effect. Therefore, the benefit of the leading-edge flap increases on the configuration with the trailing-edge flap deflection as compared with no trailing-edge flap deflection. Thus, the drag reduction by the leading-edge flap with the trailing-edge flap
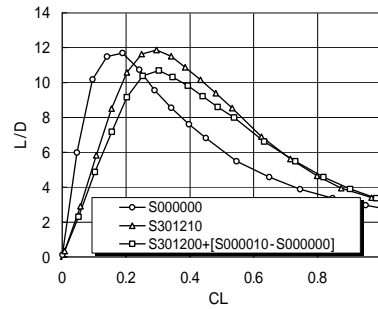

Fig.5 The synergy effects of the leading-edge and the trailing-edge

deflection is larger than that without the trailing-edge flap deflection.

The averaged velocity vector and the *u*-velocity contour measured by the PIV are plotted on a plane normal to the body axis at different chordwise locations in Fig.6. An inboard leading-edge separation vortex and an outboard leading-edge separation vortex are observed on the upper surface of the *S000000* in Fig.6(a), while, no vortex or very weak vortices are observed on the *S301200* in Fig.6(b). The inboard leading-edge flap and the outboard leading-edge flap can restrict the vortices formations. These flap performances induce the decrease in the drag.

In this section, the performances of the leading-edge and trailing-edge flaps have been made clear on the longitudinal aerodynamics. These flaps improve the lift-to-drag ratio of the wing at relatively high C_L range greater than 0.3.
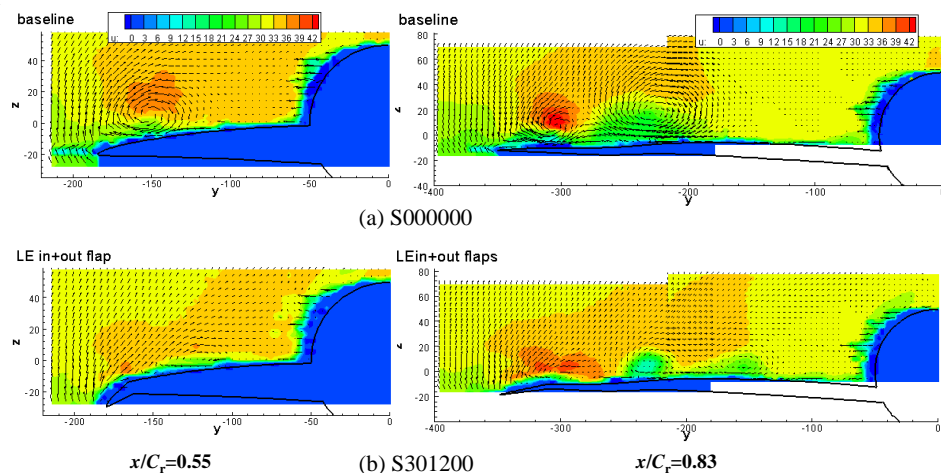

(a) S000000

(b) S301200

Fig.6 Averaged velocity vectors and streamwise velocity contour at x/C_r=0.55 and 0.83

3.2 Rolling Moment Characteristics with LE Flap and TE Flap

Static rolling moment characteristics of the SST configuration with the inboard and outboard leading-edge (LE) flaps and the trailing-edge (TE) flap are summarized in this section.

3.2.1 Baseline configuration
Before discussing the leading-edge and trailing-edge flap performances on roll characteristics, the rolling moment characteristics on the baseline configuration (*S000000*) is briefly summarized [14].

Figure 7 shows the static rolling moment characteristics at several incidence angles of σ. With increasing the roll angle of the model, linearly stable (restoring) rolling moments act to the model at low incidence angles when σ =12 and 16°. Drastic changes of rolling moments from a stable state to an unstable one are observed at an incidence angle of σ =20 degrees when the roll angle ϕ is greater than 10°. Figure 8 shows averaged velocity vectors and the *u*-velocity contours at x/c_r=0.83 for different roll angles at σ=20°. Formation of the inboard and outboard vortices is clearly observed in this figure. This figure indicates the enlargement of the area where *u* is nearly 0m/s inside the inboard vortex on the windward wing, as the roll angle is increased. This area corresponds to the one where the vortex has broken down. On the other hand, shrinking of the area where *u* is nearly 0m/s in the inboard vortex on the leeward wing is observed when ϕ=-20°. This is caused by a movement of the vortex breakdown chordwise location towards the wing apex on the windward wing and toward the trailing-edge on the leeward wing. This asymmetric chordwise movements of inboard vortex breakdown on the leeward and windward wings produces a drastic
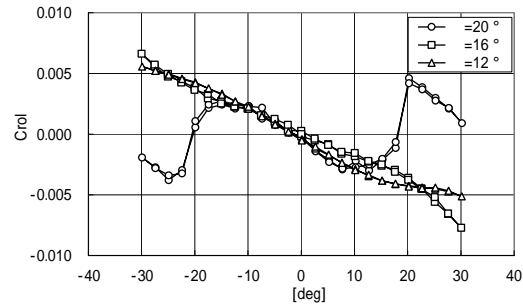

Fig.7 Rolling moment characteristics at different incidence angles

change in rolling moments.. Detail rolling moment characteristics on the baseline configuration was discussed in reference [14].

3.2.2 Leading-edge flaps
In this sub-section, rolling moment characteristics of the following three configurations are discussed as compared with the baseline configuration *S000000* [12]. 1) *S300000*: the configuration with the inboard leading-edge vortex flap deflection of 30°. 2) *S001200*: that with the outboard leading edge flap deflection of 12° and 3) *S301200*: the inboard and outboard leading-edge flaps deflection at the same time. Figure 9 shows
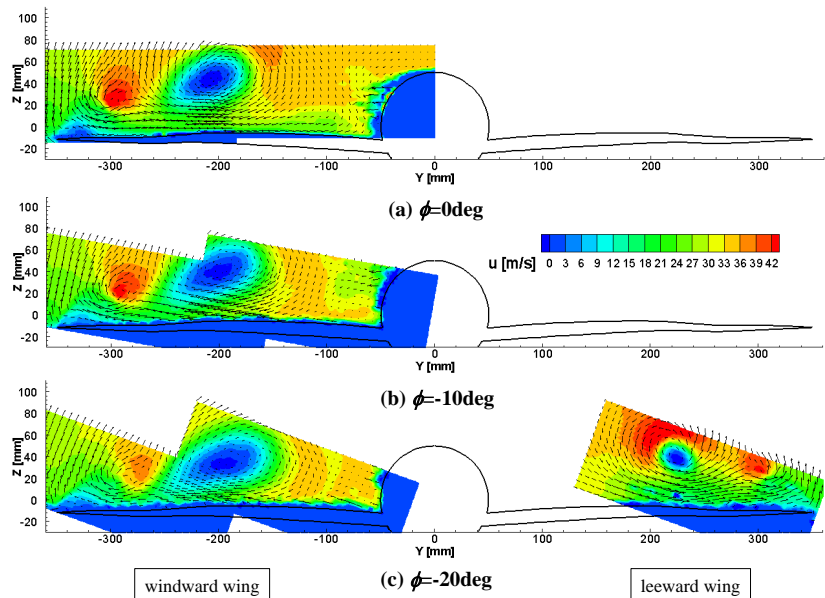

Fig.8 Averaged velocity vectors and streamwise velocity contour at different roll angles on the baseline configuration (=20deg, x/cr=0.83)

6

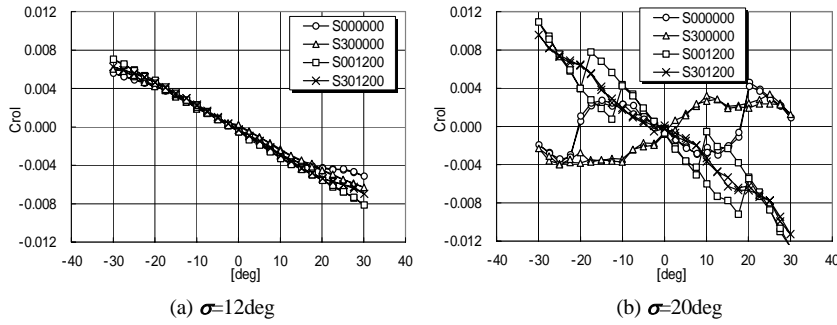(a) σ=12deg　　　　　(b) σ=20deg

Fig.9 Rolling moment characteristics with or without flap deflection

(a) x/c_r=0.55　　　　　(b) x/c_r=0.83

Fig.10 Local rolling moments with or without flap deflection
(σ=20deg)

(a) windward　　　　　(b) leeward
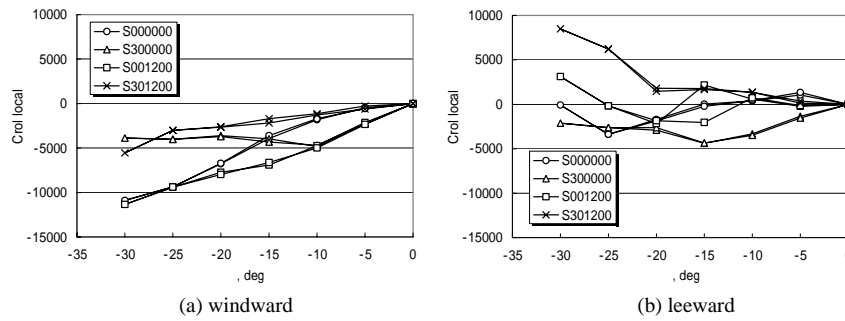
Fig.11 Local rolling moments with or without flap deflection
(σ=20deg, x/c_r=0.83)

static rolling moment curves at σ=12° and 20° when these configurations are rolled statically. Relatively linear and stable rolling moment coefficients are observed for all the tested configurations at σ=12°, whereas different rolling moment characteristics can be seen at σ=20°. When the model is rolled from ϕ=0° to ϕ=30° statically, unstable rolling moment is observed on the *S300000* for the whole range of ϕ. The hysteresis of the C_{rol} at about ϕ=10°- 20° is observed on the *S001200*. The C_{rol} indicates a closed circle rotating to counter clockwise direction. Relatively stable and linear C_{rol} curve is again observed on the *S301200*. No hysteresis and no unstable region are observed for this configuration.

Surface pressure measurements have been made for these rolled configurations. By using these results, we discuss spanwise distributions of local rolling moment components. To analyze the measured static pressure (C_p) distributions on the left wing, an assumption was made that similar flow is realized on the right wing when the wing model has an positive roll angle ($\phi_p > 0°$) and on the left wing when the model has a negative roll angle ($\phi_n = -\phi_p$) [12]. This assumption also makes us possible to obtain rolling moment components from the upper surface C_p distributions on the left wing. Next, we discuss local rolling moment component ($C_{rol\ local}$) that was obtained both from upper surface C_p distributions on the right ($C_{p\ right}$) and those on the left wing ($C_{p\ left}$) at each chordwise location. When the wing model is rolled in negative roll direction, if the value of $C_{rol\ local}$ (see Eq.(1)) is positive, C_p distributions at this chordwise location contribute to stabilize the rolling moment acting on the wing. On the other hand, when it is negative, C_p distributions contribute to unstabilize the rolling moment acting on the wing. The magnitude of the $C_{rol\ local}$ values also means the strength of the roll stability. Therefore the contribution of C_p
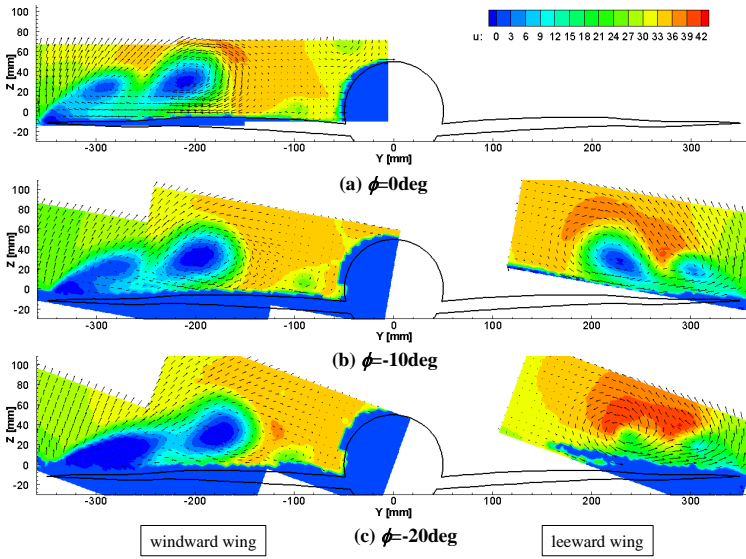
(a) ϕ=0deg

(b) ϕ=-10deg

windward wing   **(c)** ϕ=-20deg   leeward wing

Fig.12 Averaged velocity vectors and streamwise velocity contour at different roll angles on the "*S300000*" (=20deg, x/c$_r$=0.83)

(a) *clockwise direction (CW)*

(b) *counter clockwise direction (CCW)*

Figure 13. Hysteresis of the chordwise burst position on the inboard leading edge vortex on the "*S001200*" (ϕ=-15deg)

distributions to the roll stability can be understood from $C_{rol\ local}$ at a chordwise location.

$$C_{rol\ local} = \int_{root}^{LE} (C_{p\ left} - C_{p\ right})\ y\ dy \qquad (1)$$

Figure 10 shows the $C_{rol\ local}$ at several roll angles for each model configurations at σ=20° when the model is rolled in the negative direction. All configurations have positive or very small negative values at x/c_r=0.55 (Fig.10(a)). This means that the C_p distributions at x/c_r =0.55 mainly contributes to stabilize the rolling moment. Whereas, in Fig.10(b), most of values of $C_{rol\ local}$ at x/c_r=0.83 except *S301200* which indicated positive static stability have negative values. The local span length at x/C_r=0.83 is longer than that at x/C_r =0.55, thus contribution to the rolling moment at x/C_r =0.83 is higher than that at x/C_r=0.55. When the $C_{rol\ local}$ distributions (Fig.10(b)) are compared with C_{rol} characteristics (Fig.9), it is seen that both results qualitatively agree well except *S001200*.

To clarify the local contributions of C_p distributions at x/c_r =0.83 to the rolling moments, the results of $C_{rol\ local}$ (Fig.10(b)) are divided into contributions from the leeward
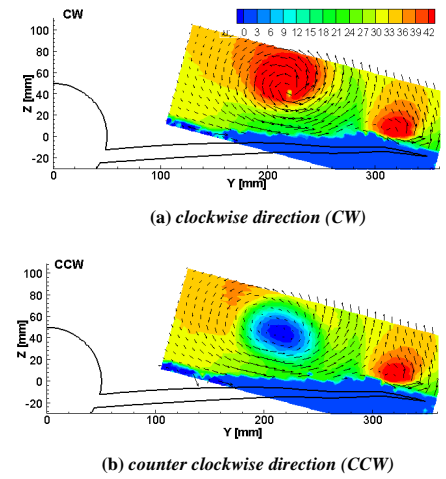
wing side (right wing) and those from the windward wing (left wing) when the wing model is rolled in the negative direction (Fig.11). The $C_{rol\ local}$ on the windward wing at x/c_r=0.83 has negative value for most of the results, thus contributing to unstabilize the rolling moment acting on the wing for all the model configurations. However, the $C_{rol\ local}$ distributions on the leeward wing at x/c_r=0.83 indicate nonlinear-like behaviors. The *S001200* indicates different sign of $C_{rol\ local}$ at about ϕ=-20°. This suggests that the hysteresis of the $C_{rol\ local}$ on the *S001200* is induced by the C_p distributions on the leeward wing. The $C_{rol\ local}$ on the leeward wing of the *S300000* shows strong contribution to the unstable rolling moments as compared with other three configurations. Similar discussion can be made for other configurations. The distributions of *S301200* indicate strong contribution to stabilize the rolling moment. Those of the *S000000* indicate destabilized effect when ϕ<-20° and stabilized effect when ϕ>-20°. These characteristics corresponds to those shown in Fig.9(b). Therefore, the rolling moment characteristics (Fig.9) at σ=20° are depended on

the flow patterns over the leeward wing at x/c_r=0.83.

Figure 12 shows averaged velocity vectors and the u-velocity contour at different roll angles at x/c_r=0.83 of σ=20°. Both the inboard and outboard leading edge separation vortices have already been broken down at ϕ=0° on $S300000$, because the u-velocity component u is nearly 0m/s for all vortices formed on the wing. At ϕ=-20°, inboard and outboard vortices on the leeward wing do not indicate the sign of vortex breakdown These behaviors of the inboard and outboard vortices on the leeward and windward wings contribute to unstabilize rolling moment acting on the wing. Therefore unstable rolling moment was obtained on the $S300000$ (Fig.9(b)).

Figure 13 shows averaged velocity vector distributions on the leeward wing at ϕ=-15°. Although both results in Fig.13(a) and Fig.13(b) were measured at the same roll angle (ϕ=-15°), the measured history of the roll angle for both results is different. Fig.13(a) was measured after the wing model was rolled from ϕ=-20° to ϕ=-15° ("clockwise direction"), The Fig.13(b) was obtained after the wing model was rolled from ϕ=-10° to ϕ=-15° ("counter clockwise direction"). When the case of the "clockwise direction" is compared with the case of the "counter clockwise direction", behaviors of the inboard leading edge separation vortex are different each other. The concentrated inboard vortex is formed in the case of "clockwise direction", while the inboard vortex that has already been broken down in case of "counter clockwise direction". As discussed in Fig.11, behaviors of the inboard vortex on the leeward wing have strongly affected the $C_{\rm rol}$ distributions. Thus, we can conclude that the rolling moment hysteresis on the $S001200$ is depended on the vortex breakdown characteristics on the leeward wing.

The $S000000$ and the $S001200$ have the same inboard leading edge configurations but the
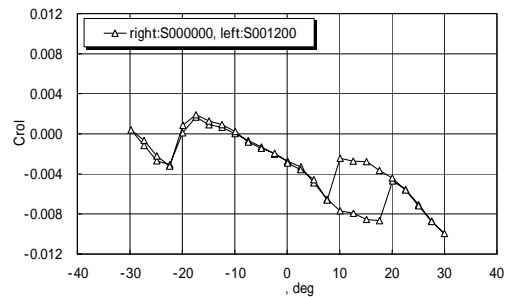

Fig.14 Asymmetric Leading-edge flap deflection (σ=20deg)

different outboard leading-edge flap deflection angles. However, as was shown in Fig. 9b), the rolling moment hysteresis is observed on the $S001200$, but not on the $S000000$. As discussed in reference [12], the distance from the center of the inboard vortex to the center of the outboard vortex on the $S001200$ is larger than that of the $S000000$. Therefore, interaction between the inboard and outboard vortices on the $S001200$ is weaker than that on the $S000000$. The behavior of the inboard vortex interacting with the outboard vortex will be influenced by the behavior of the outboard vortex. Static hysteresis of the vortex breakdown occurrence on the delta wing was reported in reference [18]. In this reference, static hysteresis of the vortex breakdown was observed when the chordwise position of the vortex breakdown occurrence is changed very near the wing trailing edge. Flow conditions are different between those over the wing surface and that aft part from the trailing edge. Therefore, different behaviors of vortex breakdown are observed between when breakdown position progresses toward the apex beyond the trailing edge and when that position retreats to the aft part of the trailing edge. The
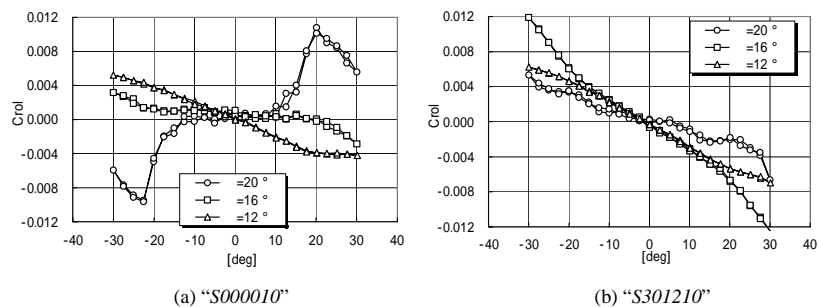

(a) "S000010"

(b) "S301210"

Fig.15 Rolling moment characteristics with or without trailing-ege flap deflection

hysteresis of vortex breakdown that was observed on the *S001200* is very similar to that observed on the delta wing in [18]. Although the behavior of the inboard vortex breakdown is influenced by the outboard vortex, no hysteresis was observed on the *S000000*, because of the stronger interaction between the inboard and outboard vortices.

Figure 14 shows rolling moment curves at σ=20° when the right wing configuration is the *S000000* and the left wing configuration is the *S001200*. Abrupt changes of C_{rol} are observed near ϕ=-20°. When the C_{rol} on the *S000000* in Fig.9 is compared with C_{rol} in Fig.14, both results show similar trend near ϕ=-20°. The rolling moment hysteresis was also observed near ϕ=20° in Fig.14. This distribution is similar to that on the *S001200* with flaps deflected symmetrically (Fig.9). Wing configuration of the leeward wing is *S000000* when ϕ<0, but *S001200* when ϕ>0. As discussed in Fig.11, the flow over the leeward wing mainly determines the roll characteristics. From these results, it is confirmed that both the abrupt change of the C_{rol} on the *S000000* and the hysteresis of the C_{rol} on the *S001200* are induced by the different breakdown behaviors of the inboard vortices on the leeward wing..
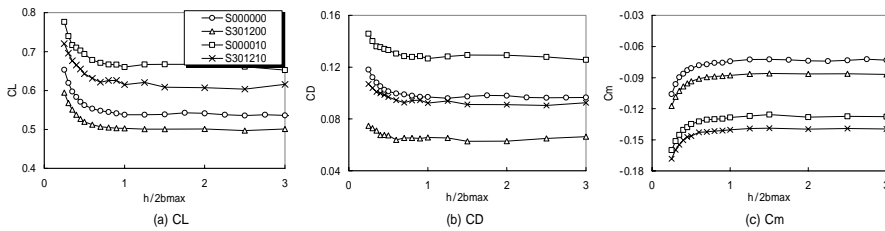
3.2.3 Trailing-edge flap

Figure 15 shows the C_{rol} vs. ϕ curves for the configuration with the trailing-edge flap deflection (*S000010*) and the one with the leading-edge and trailing-edge flaps deflection (*S301210*). For *S000010*, the linear and stable rolling moment is observed at σ=12° that is similar to that on the *S000000*. With increasing the incidence angles to σ=16° and 20°, overall distributions of the C_{rol} are similar to the *S000000*, while the magnitude of the static stability is decreased as compared with the *S000000*. Similar tendency is observed in the C_{rol} curves for the *S301210* in Fig.15(b) and for the *S301200* in Fig.9. The trailing-edge flap increases the effective angle of attack, thus there are possibilities promoting the vortex breakdown near the trailing-edge. At relatively low incidence angles, vortex breakdown does not occur on the wing. Therefore, even though the trailing-edge flap is deflected, vortex breakdown usually does not occur. However, at high incidence angle, the trailing edge may promote the occurrence of the vortex breakdown then the instability component of the rolling moment will be increased as compared with the configuration without trailing-edge deflection. These explain that the stability of the rolling moment is slightly decreased by the trailing-edge flap deflection at relatively high incidence angle as was observed in Fig.15.

3.3 Ground Effects with LE Flap and TE Flap

The performances of the leading-edge and trailing-edge flaps with the ground effects are summarized in this section. Figure 16 shows the C_L, C_D and C_m curves for the *S000000*, *S301200*, *S000010* and *S301210* when the models are moved toward the ground statically at α=12.5° and when ϕ=0°. The lift,

Fig.16 Ground effects on the configurations with or without leading-edge and trailing-edge flap deflections (α=12.5deg)

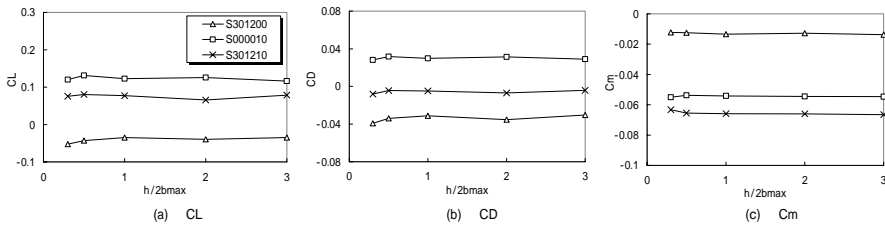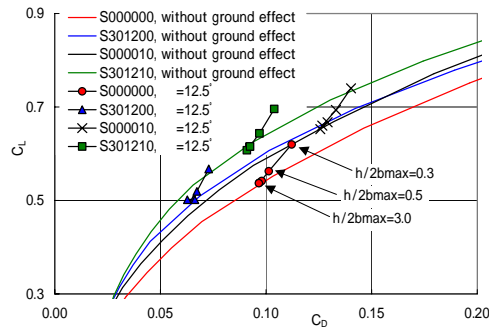Fig.17 Change of the forces and moment induced by the ground effect (α=12.5deg)

Fig.18 Drag polar performances of the leading-edge and the trailing-edge flap with the ground effect (α=12.5deg)

Fig.19 Ground effect on the rolling moment characteristics (*S000000*)

drag and nose-down pitching moment are increased by the ground effect as the height from the ground $h/(2b_{max})$ decreases to 0.25. Similar tendencies are observed for all four configurations tested. The ground effects can be observed when the model is lower than $h/(2b_{max})$=1.0. The difference ΔC_L between the lift of the configuration with a flap deflection and that of the baseline configuration at each $h/(2b_{max})$ are plotted in Fig.17(a) to make clear the flap performance within the ground effects. The differences of the drag and the pitching moment (ΔC_D and ΔC_m) are similarly obtained and plotted in Figs.17(b) and (c). At most of $h/(2b_{max})$, these three are almost constant and only a slight change of the ΔC_L, ΔC_D and ΔC_m are observed at $h/(2b_{max})$<0.5. The effects of the leading-edge and trailing-edge flaps on the ground effect is very small.

Figure 18 shows C_L vs. C_D values for the four configurations at several $h/(2b_{max})$. The drag polar curves without ground effect are also plotted in Fig.18. The ground effects induce the increase in the lift and drag as was seen in Fig.16. As for *S000000*, the trajectory of the C_L-C_D curves when the model approaches toward the ground is not corresponding with the C_L-C_D curves obtained by altering angles of attack without ground effect (solid line in Fig.18), i.e. higher L/D ratio is obtained for the model within the ground effect. It suggests that the ground effect not only increases the effective angle of attack but also increases the effective wing aspect ratio. The same tendency is
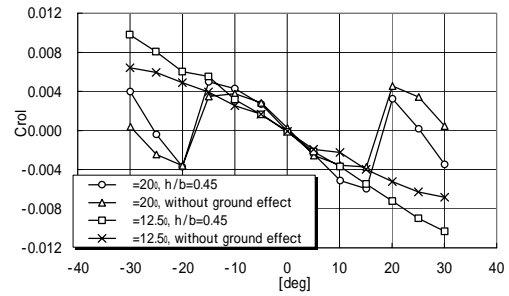
observed for the configurations with the leading-edge and trailing-edge flaps deflection. The ground effect increases the nose-down pitching moment as was seen in Fig. 16. Therefore, the longitudinal stability becomes more stable. Figure 19 shows the rolling moment curves on the baseline configuration with and without ground effect at σ=12.5° and 20°. This figure indicates the ground effects on the SST model contributes to increase roll stability as compared with that without ground effect.

4 Conclusions

Low-speed and high angle of attack aerodynamics were investigated to improve the take-off and landing performance of the SST configuration. Wind tunnel tests were conducted on an SST model with the leading-edge and trailing-edge flaps. Performances of the leading-edge and trailing-edge flaps were investigated for 1) the lift-to-drag ratio, 2) the rolling moment characteristics and 3) the ground effect. When the leading edge and trailing edge flaps are deflected at a same time, obvious improvement of the lift-to-drag ratio was obtained. This improvement is larger than the sum of each benefit with the leading edge flap and the trailing edge flap deflected independently. Different rolling moment characteristics was observed for the configurations with and without flap deflection at high incidence angle, whereas linear and statically stable rolling moment characteristics were obtained for all the configurations at low

11

incidence angles. The ground effects contribute to increase the lift-to-drag ratio. These flap performances were only slightly affected by the ground effects. The static stability of the rolling moment characteristic was also increased by the ground effect.

References

[1] Sakata K. Supersonic Experimental Airplane (NEXST) for Next Generation SST Technology - Development and Flight Test Plane for the Unmanned Scaled Supersonic Glider-, Reno, USA, AIAA Paper 2002-0527, 2002.

[2] Yoshida K and Makino Y. Aerodynamic Design of Unmanned and Scaled Supersonic Experimental Airplane in Japan, Finland, ECCOMAS 2004.

[3] Rinoie K and Stollery J L. Experimental studies of vortex flaps and vortex plates, *Journal of Aircraft*, Vol. 31, No. 2, 1994, pp. 322-329.

[4] Terry T, Malcolm G N and Lewis L C. Experimental Study of Vortex Flows over Delta Wings in Wing Rock Motion, *Journal of Aircraft*, Vol.29, No.4, 1992, pp.598-603.

[5] Hummel D and Srinivasan P S. Vortex Breakdown Effects on the Low-Speed Aerodynamic Characteristics of Slender Delta Wings in Symmetrical Flow, *Journal of Royal Aeronautical Society*, Vol.71, 1967, pp.319-322.

[6] Wentz W H and Kohlman D L. Vortex Breakdwon on Slender Sharped-Edged Wings, *Journal of Aircraft*, Vol.8, No3, 1971, pp156-161

[7] Brennenstuhl U and Hummel D. Vortex Formation Over Double-Delta Wings, Proceedings of 13th Congress of the International Council of the Aeronautical Science (ICAS Paper 82-6.6.3), Seattle, USA, Aug. 1982, pp 1302-1309.

[8] Kwak D Y. Unsteady Aerodynamic Characteristics on Rolling Delta Wings, *Journal of Japan Society for Aeronautical and Space Sciences*, Vol.47, No.543, 1999, pp.165-173 (in Japanese)

[9] Sato J, Fujii K, Umezawa D and Sunada Y. Experimental Aerodynamics on Rolling Delta Wing at High Angles of Attack, *Fluid Dynamics of High Angle of Attack*, Spring-Verlag, Berlin, 1992, pp.425-439.

[10] Chang R C and Muirhead V U. Effect of Sink Rate on Ground Effect of Low-Aspect-Ratio Wings, *Journal of Aircraft*, Vol.24, No.3, 1987.

[11] Rinoie K, Miyata K, Kwak D Y and Noguchi M. Studies on Vortex Flaps with Rounded Leading-Edges for Supersonic Transport Configuration, *Journal of Aircraft*, Vol.41, No.4, 2004, pp.829-838.

[12] Kwak D Y, Shirotake M, Rinoie K, Watanabe S and Kato H. Roll Characteristics of an SST Configuration with Leading Edge Flaps at High Alpha, AIAA Paper 2004-5082, Aug.2004.

[13] Fujita T, Iwasaki A, Fujieda H, Shigemi M, Nakayasu H and Sagisaka M. Model Support System Using an Industrial Robot in Low-speed Wind Tunnel, National Aerospace Laboratory Technical Memorandum, NAL-TM 666, 1994 (in Japanese)

[14] Kwak D Y, Noguchi M, Shirotake M and Rinoie K. Rolling Moment Characteristics of Supersonic Transport Configuration at High Incidence Angles, *Journal of Aircraft*, accepted for publication.

[15] Nonaka O, Kayaba S and Hayahi Y. Moving belt ground effect testing System of NAL 6.5×5.5m Low Speed Wind Tunnel, National Aerospace Laboratory Technical Memorandum NAL-TM 724, 1998 (in Japanese)

[16] Watanabe S, Kato H, Kwak D Y, Shirotake M and Rinoie K. Stereo PIV Measurements of Leading Edge on a Cranked Arrow Wing, *Measurement Science and Technology*, Vol.15, No.6, 2004, pp1079-1089.

[17] Kwak D Y, Miyata K, Noguchi M and Rinoie K. Lift-to-Drag Ratio Improvement of a Supersonic Transport with Leading-Edge and Trailing-Edge Flaps, *Journal of Japan Society for Aeronautical and Space Sciences*, Vol.51, no.597, 2003, pp.551-558(in Japanese)

[18] Jobe C E, Hsia A H, Jenkins J E and Addington G A. Critical States and Flow Structure on a 65-Deg Delta Wing, *Journal of Aircraft*, Vol.33, No.2, 1996, pp.347-352.